J. Fluid Mech. (1970), *vol.* 41, *part* 2, *pp.* 241–258
Boeing Symposium on Turbulence

The mechanics of an organized wave in turbulent shear flow

By A. K. M. F. HUSSAIN AND W. C. REYNOLDS
Department of Mechanical Engineering, Stanford University

(Received 2 September 1969)

Some preliminary results on the behaviour of controlled wave disturbances introduced artificially into turbulent channel flow are reported. Weak plane-wave disturbances are introduced by vibrating ribbons near each wall. The amplitude and relative phase of the streamwise component of the induced wave is educed from a hot wire signal, allowing the wave speed and attenuation characteristics and the wave shape to be traced downstream. The normal component and wave Reynolds stress have been inferred from these data. It appears that Orr–Sommerfeld theories attempted to date are inadequate for description of these waves.

1. Introduction

There is considerable current interest in the possibility of representing shear flow turbulence as a random superposition of appropriate characteristic waves. Two distinct but related views have been suggested. In Lumley's (1967) orthogonal decomposition the waves are effectively marginally stable and strongly coupled through their non-linear interactions. In contrast, Landahl's (1967) wave representation involves waves that are born at some location and decay as they proceed downstream. Landahl's waves might be viewed as the Fourier components of Lumley's (1967) characteristic eddies. Which representation is the more useful remains to be determined. However, a satisfactory closed equation system for the wave eigenfunctions has not yet been found in either case, and, as Landahl suggests, experiments are sorely needed at this point. The primary objective of the present work is the acquisition of appropriate data and the continued development of these ideas.

There are two basic ways to approach the experimental problem. One can attempt to deduce the nature of the eigenfunctions from appropriate two-point correlation data (Lumley 1967; Bakewell & Lumley 1967; Morrison & Kronauer 1968). Alternatively, one can seek the same result by systematic controlled perturbations of the basic turbulent shear flows. Indeed, a considerable body of data on the closely related problem of turbulent shear flow over a waving boundary is just becoming available (Kendall, private communication; Stewart, private communication). Such studies treat boundary-value problems involving the wave eigenfunctions. Another approach is to introduce the controlled disturbance within the fluid at some point, and then to study the behaviour of this disturbance

downstream. This initial-value problem leads one directly to decaying eigenmodes of the Landahl type. The present paper describes initial output from just such an experiment.

With this background of motivation, let us now turn to the simple problem of the behaviour of an organized wave in a turbulent shear flow. We can imagine the wave as being introduced by an upstream wave-maker. We can use the cyclic position of the wave-maker as a clock for selective sampling, which permits us

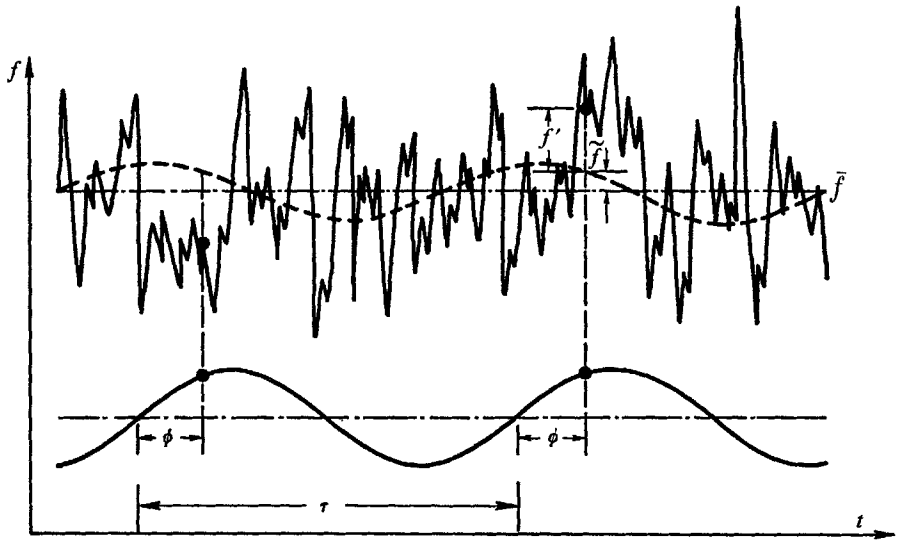

FIGURE 1. The time and phase averages of a random signal with a weak organized wave. Sketch shows the procedure for obtaining phase average of the signal (upper curve) at phase ϕ of the reference signal (lower curve). Time average $\equiv \bar{f}$, phase average $\equiv \langle f \rangle = \bar{f}+\tilde{f}$.

to extract the (weak) organized wave motion from a background field of finite turbulent fluctuations. In the presence of such travelling waves, we can decompose any fluctuating quantity $f(x,t)$ as (figure 1)

$$f(\mathbf{x},t) = \bar{f}(\mathbf{x}) + \tilde{f}(\mathbf{x},t) + f'(\mathbf{x},t); \tag{1.1}$$

$\bar{f}$ is the mean value, $\tilde{f}$ the (statistical) contribution of the organized wave, and f' the turbulence. The time average is

$$\bar{f}(\mathbf{x}) = \lim_{T\to\infty} \frac{1}{T}\int_0^T f(\mathbf{x},t)\,dt; \tag{1.2}$$

we also define the *phase average* as

$$\langle f(\mathbf{x},t)\rangle = \lim_{N\to\infty} \frac{1}{N}\sum_{n=0}^{N} f(\mathbf{x},t+n\tau), \tag{1.3}$$

where τ is the period of the wave (wave-maker). The phase average is then the average, at any point in space, of the values of f that are realized at a particular phase ϕ in the cycle of the wave-maker. The wave component $\tilde{f}$ is then

$$\tilde{f} = \langle f\rangle - \bar{f}. \tag{1.4}$$

Hence, given a signal $f(t)$ at some particular location, and given a reference signal oscillating at the wave frequency (the wave-maker displacement), the three components of f can be determined by appropriate signal analysis. Some useful properties that follow from the basic definitions are given below.

$$\left.\begin{aligned} &\langle f' \rangle = 0, \quad \tilde{f} = 0, \quad \bar{f}' = 0, \quad \langle \bar{f} \rangle = \langle \tilde{f} \rangle = \bar{f}, \\ &\langle \tilde{f} q \rangle = \tilde{f} \langle q \rangle, \quad \langle \bar{f} q \rangle = \bar{f} \langle q \rangle, \quad \overline{\langle \tilde{f} q' \rangle} = \overline{\tilde{f} q'} = 0. \end{aligned}\right\} \tag{1.5}$$

The last of these states that, on the average, the background turbulence and the organized motion are uncorrelated.

One can proceed by suitable manipulation with the Navier–Stokes equations to obtain equations governing $\tilde{u}_i, \tilde{P}$ for a particular wave (Phillips 1967). These equations are not closed, for they contain terms involving the oscillations ($\tilde{r}_{ij}$) in the Reynolds stresses of the background turbulence,

$$\tilde{r}_{ij} = \langle u_i' u_j' \rangle - \overline{u_i' u_j'}. \tag{1.6}$$

This lack of closure necessitates an empirical closure of some sort. Experiments hopefully will provide the basis for a satisfactory closure assumption.

In this paper we shall describe the apparatus used for our experiments in some detail, document the basic flow, present certain preliminary wave results, and report without documentation the outcome of a few attempts to predict the wave structure with various closure assumptions. More detailed data and analysis will follow in subsequent publications.

2. Experimental apparatus

Theoretical models cope most readily with parallel flows; hence a two-dimensional channel flow forms the basis for our experiments. A schematic of the channel is shown in figure 2.† Previous channel experiments (Laufer 1951; Comte-Bellot 1963; Clark 1968) indicated clearly that a very long flow length was necessary to achieve full development of the Reynolds stress profiles. Believing that this is due in part to the persistence of large eddies originating upstream of the channel, special care has been taken to prevent large-scale motions from entering the channel, early development of the mean field has been assisted, and a long region is provided for development of the turbulence field.

The gap width is 2·5 in., and the channel cross section has an aspect ratio of 18:1 and a length/gap ratio of 230:1.

The entrance section is fabricated from heavy plywood with wood bracings and metal end spacers. Distortions in the entrance region due to temperature and humidity-sensitive warpage are less than $\pm 0{\cdot}025$ in. on the local gap, and the entire surface is hydraulically smooth. The primary test section wall has an unpenetrated surface of smooth formica on a rigid particle board base, and is flat to within $\pm 0{\cdot}005$ in. The opposing wall is wood-braced lucite, and remains flat to within $\pm 0{\cdot}005$ in. Instrumentation and wall pressure taps are passed through the lucite side wall, which permits ready observation for probe location purposes. The channel operates at a pressure slightly above

† See Hussain (1970) for more detail.

atmospheric, with blown air supplied from a large filtering plenum (98% retention to 0·7 μ). A screen minimizes disturbance reflexions where the test section discharges into the laboratory. Excitation through mechanical vibration is suppressed. Flow pulsations are minimized through use of a constant-speed motor, a lightly loaded blower, and a high series flow resistance.

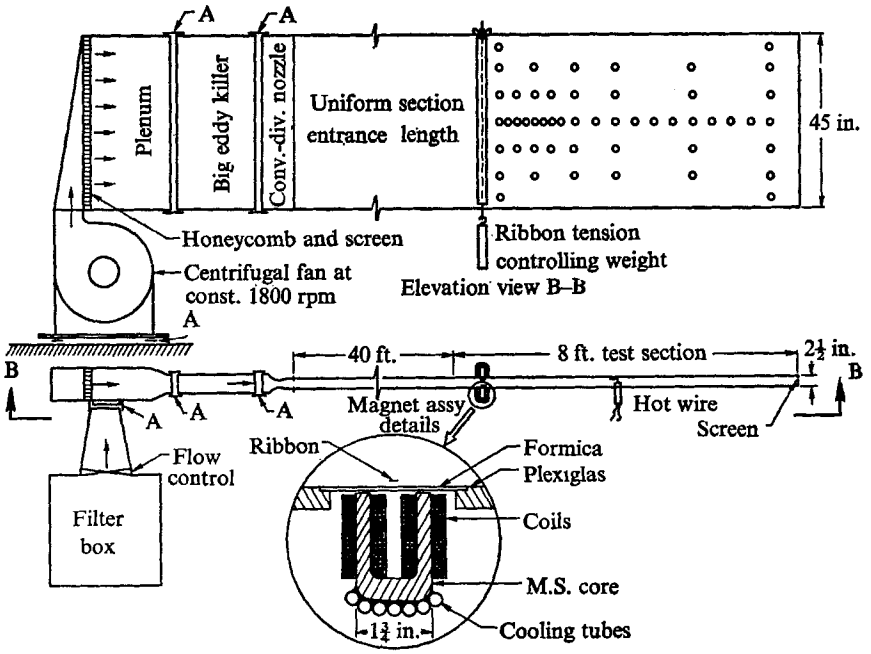

FIGURE 2. The channel. A: flexible rubber connexion. Circles denote probe survey stations.

The controlled disturbance is introduced by two vibrating ribbons on the opposing walls at the start of the test section. The ribbons are stretched vertically across the span of the flow, and carry sinusoidal current in the presence of steady d.c. magnetic fields produced by electromagnets outside of the flow. The $\frac{3}{16}$ in. wide, 0·0035 in. thick, spring phosphor bronze ribbons are placed in tension which is adjusted to match their natural frequencies away from operating frequencies. They are located approximately $\frac{1}{16}$ in. from the walls. The ribbon current and magnet voltage are manually controlled to maintain fixed vibration amplitude within $\pm 5\%$. Stroboscopic observations confirm that the ribbons vibrate smoothly in a flutter free, torsion free cosine-like mode, with the maximum amplitude of about $\frac{1}{32}$ in. on the centre height of the channel. Hence, on the centreline the induced disturbance is essentially two-dimensional. The ribbons can be vibrated in the same direction at the same time, introducing a symmetric disturbance to the velocity component $\tilde{v}$ normal to the walls, or in opposite phase (antisymmetric $\tilde{v}$ disturbance). The disturbance velocities which can be introduced by the ribbons are typically less than 1% of the background turbulence. The instrumentation required for detection of this disturbance will be described following a documentation of the basic shear flow.

3. The basic flow

The wave experiments are performed at a channel Reynolds number (based on channel half-width δ and centreline velocity U_0) of approximately 13,800. At higher speeds ribbon flutter prevents proper oscillation. Basic flow data (with ribbons removed) have been obtained at this and higher Reynolds numbers for the purpose of apparatus qualification and flow documentation.

Mean velocity profiles were obtained with a total head probe made from 0·025 in. OD tubing (0·0025 in. wall thickness) flattened to an opening of 0·006 in. This probe was calibrated against a keil probe and was found to have a yaw plateau of $\pm$ 10°. No turbulence or wall proximity corrections have been made. Static pressures were obtained from wall taps, and have not been corrected for turbulence-induced cross-stream pressure variations. The axial pressure gradient is measured by similar pressure taps located at intervals along the centre height of the channel. The wall shear stresses τ_w on the channel centre height are deduced from this axial pressure gradient using the integrated momentum equation, which gives

$$\tau_w = -\delta \frac{dP}{dx}.$$

The fluid properties are determined as functions of the static pressure, temperature, and ambient humidity.

Spanwise surveys showed that the basic flow is two-dimensional over the central 70% (32 in.) of the span. Surveys with and without the ribbon at Re = 13,800 also showed no measurable effect of the ribbons (vibrating or stationary) on the mean velocity profile in the region of wave surveys.

Figure 3 shows the friction velocity $u_\tau = \sqrt{(\tau_w/\rho)}$ over a wide Reynolds number range. Clark's (1968) data and correlation are also shown for comparison. Our data lie slightly above Clark's correlation, but extrapolate logarithmically better to the high Reynolds number data of Comte-Bellot (1963). The discrepancies between the basic flows in these and other channels are discussed in more detail by Hussain (1970). Wave data and additional basic flow data were obtained using a Thermosystems linearized temperature-compensated constant temperature hot wire anemometer system. The wires are 0·0002 in. dia., platinum, nominally $\frac{1}{16}$ in. long, soldered to a standard Thermosystems probe with needles projecting into the flow $\frac{3}{8}$ in. ahead of the $\frac{1}{8}$ in. dia. probe stem. The wires were calibrated against a total head probe on the channel centreline in the fully developed turbulent channel flow. Turbulence effects are small ($\approx$ 2%), and no turbulence correction was made. An integrating digital voltmeter was used to obtain stable signal averages. Spectra were obtained with a Quantech analyzer using a 10 Hz bandwidth over the range 30–5000 Hz.

The mean pressure distribution along the channel centre height is linear (figure 4), indicating the rapid development of the mean field.

Figure 5 shows the mean velocity profile at Re = 13,800 in the conventional wall layer co-ordinates. No wall proximity corrections or position shifts have been incorporated. The agreement between the pitot and hot wire profiles is

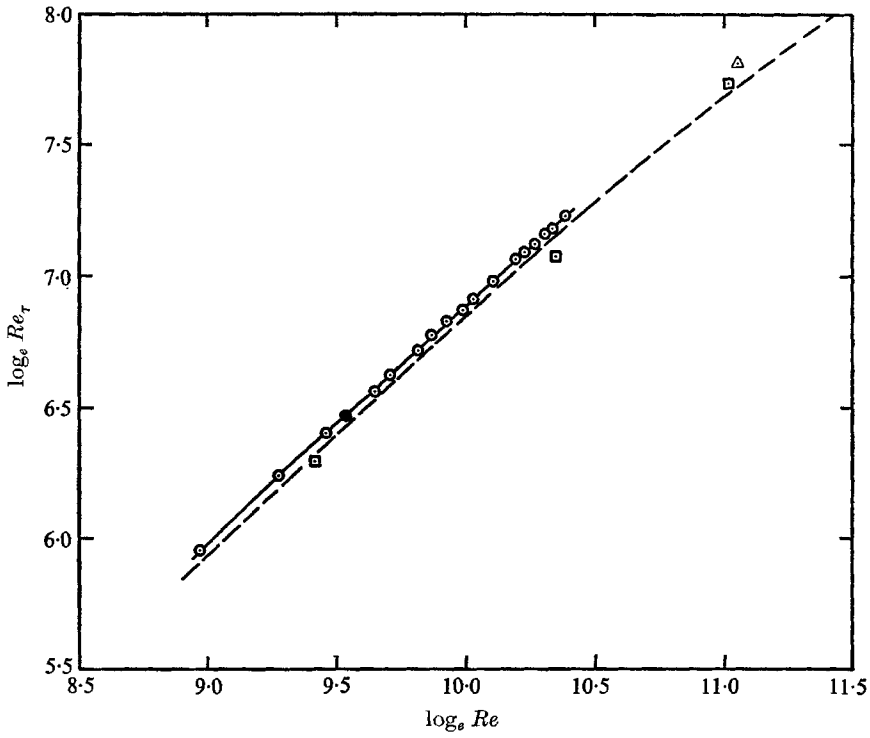

FIGURE 3. Relation between friction velocity and centreline velocity. $Re_\tau = u_\tau \delta/\nu$, $Re = U_0 \delta/\nu$. ———, best fit for Clark channel; ⊡, Laufer channel; △, Comte-Bellot channel; ●, Re = 13,800.

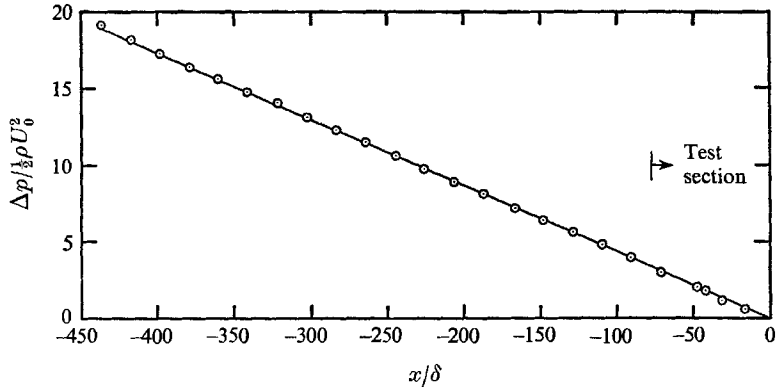

FIGURE 4. Streamwise mean pressure distribution on centre height at Re = 13,800.

excellent over the region where both techniques are accurate. This profile is in good agreement with Coles' (1956) form of the log law, though it lies below channel profiles of Laufer (1951) and Clark (1968) at comparable Reynolds numbers.

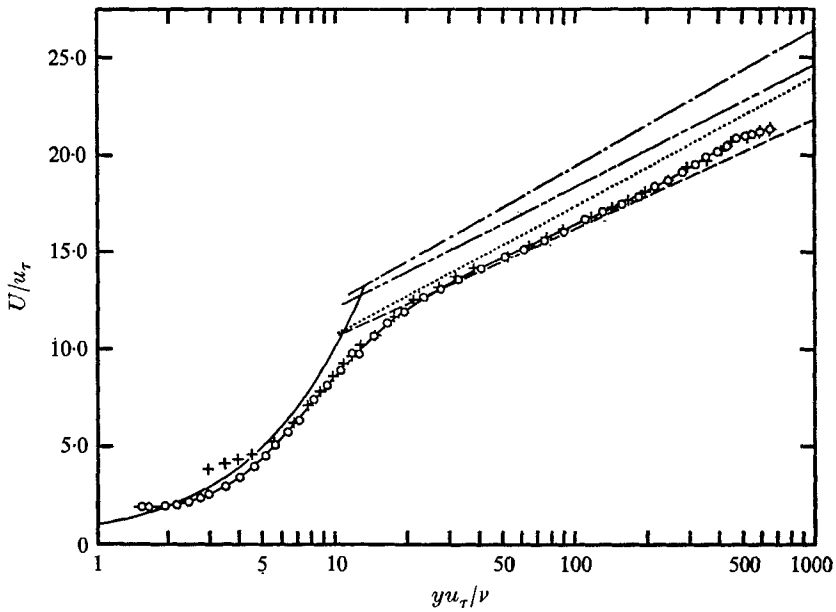

FIGURE 5. Mean velocity distribution in universal co-ordinates, Re = 13,800; ○, hot wire; +, total head probe; ——, $u^+ = y^+$; – – –, Coles's log law; ——–, Laufer, Re = 12,200 to 61,600; ....., Clark Re = 14,400; —·—, Comte-Bellot, Re = 57,000.

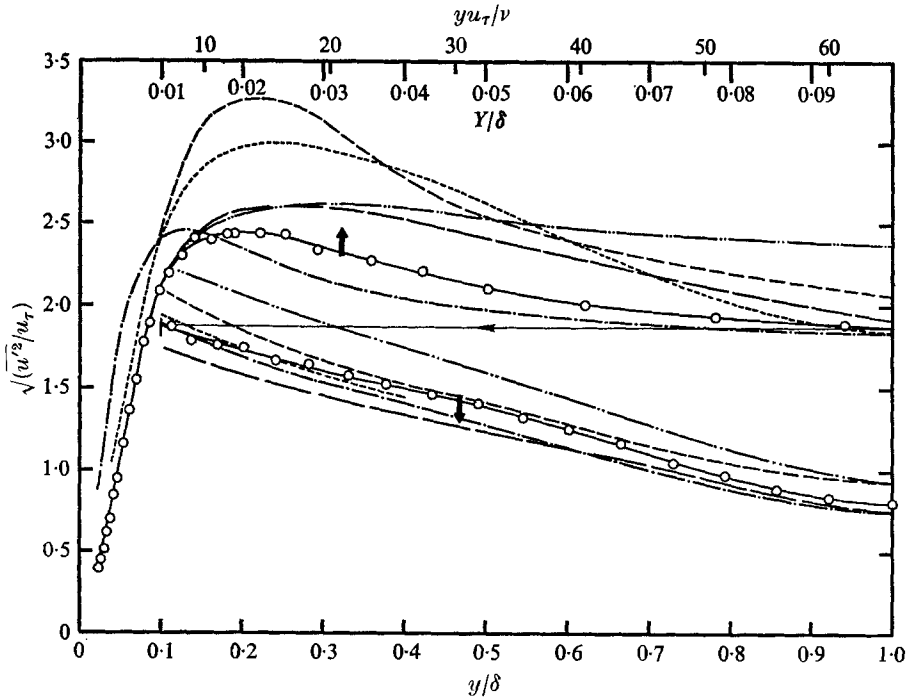

FIGURE 6. Streamwise turbulence intensity, Re = 13,800; ——, Laufer pipe, Re = 50,000; ——–, Laufer channel, Re = 30,800; – –, Clark channel, Re = 15,200. Both top scales correspond to the present experiment. Laufer channel data correspond to y/δ only, and Clark channel and Laufer pipe (radius = δ) to y^+ values only.

Figure 6 shows the r.m.s. streamwise fluctuation $\sqrt{u'^2}$ distribution at $Re = 13{,}800$. Laufer's channel (1951) and pipe (1954) data and Clark's channel (1968) data at comparable Reynolds numbers are shown for comparison.

The $\overline{u'^2}$ spectra (figure 7) show no influence of the blower wheel (30 Hz), blade (240 Hz) or a.c. supply (60 Hz) on the developed turbulent structure. For further flow documentation, and considerable basic flow data at other Reynolds numbers, see Hussain (1970).

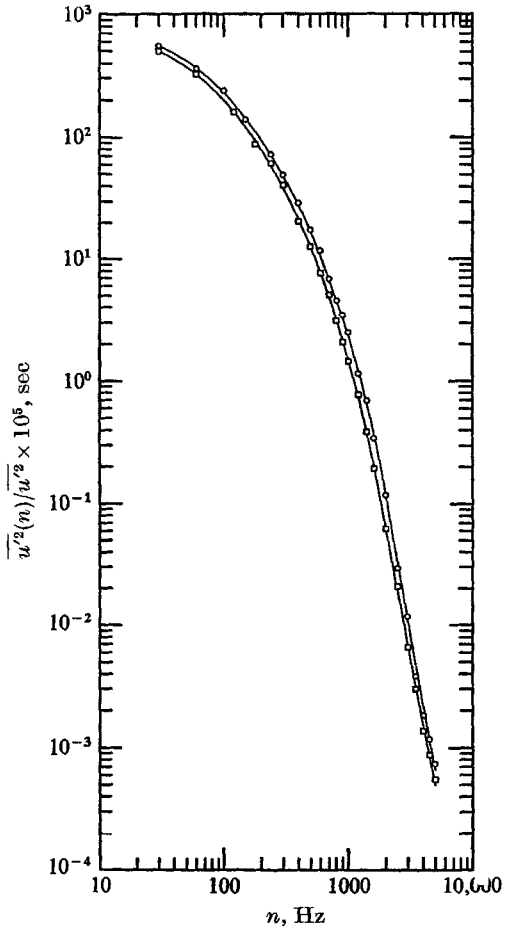

FIGURE 7. Frequency spectra of $\overline{u'^2}$ at $Re = 13{,}800$. 10 Hz bandwidth. □, $y/\delta = 0{\cdot}040$; ○, $y/\delta = 1{\cdot}0$.

4. Signal analysis apparatus

The linearized hot wire signal was processed electronically to recover the mean, wave, and r.m.s. turbulence components for streamwise fluctuations. The basic element in the system (figure 8) in a Princeton Applied Research (PAR) wave form eductor. Given a suitable periodic reference signal (the sinusoidal ribbon

voltage in the present experiment), this device samples the hot wire signal at 100 points sequentially in each cycle of the reference signal, repeats this sequential sampling in each successive cycle of the reference signal, and thereby essentially obtains an average over a very large ensemble of wave cycles. An ensemble size of 50,000 to 100,000 was necessary in these experiments. This provides the first stage of detection of the very weak wave component from the

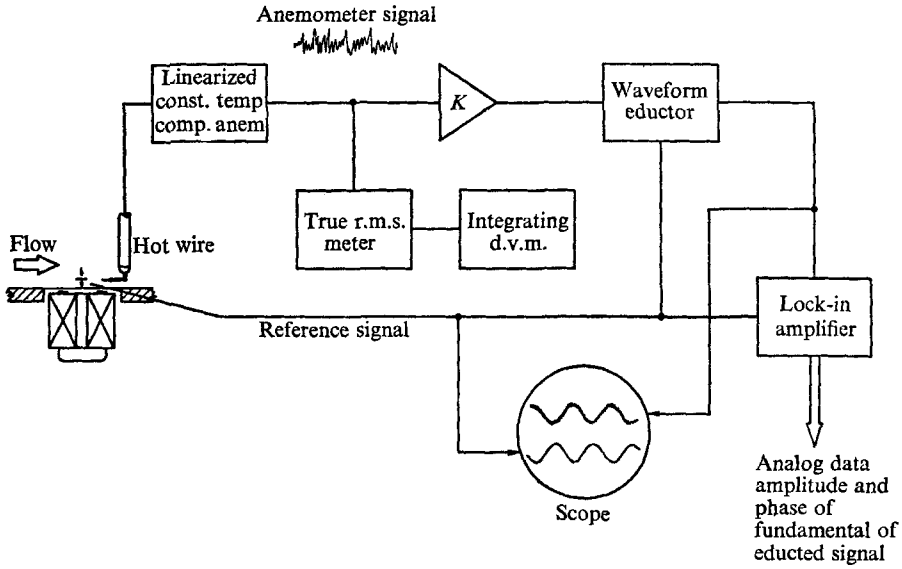

FIGURE 8. Schematic diagram of the analogue system for signal processing. Upper scope trace shows educed waveform, lower shows reference. K = 20–50.

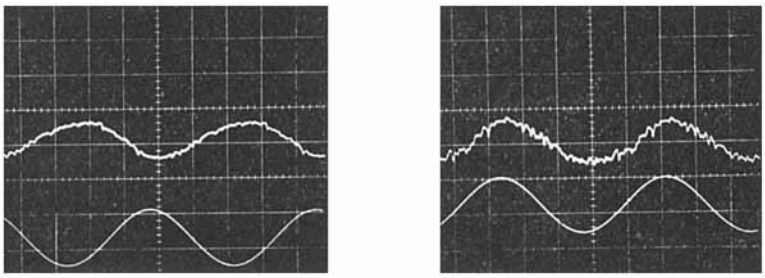

FIGURE 9. Educted signal (upper) and reference signal (lower). The hot wire signal totally masks the weak wave and is not shown. (*a*) y/δ = 0·12, wave amplitude = 0·067 ft./sec, phase = 150°. (*b*) y/δ = 0·32, wave amplitude = 0·0266 ft./sec, phase = −24°.

relatively high amplitude turbulent noise. The educed waveform can be displayed on an oscilloscope (figure 9) and still contains some noise. Further noise rejection is obtained by processing the display signal through a PAR lock-in amplifier (LIA). This device detects the amplitude and phase of a sinusoidal signal buried in noise by maximizing the quadrature against a phase-shifted sinusoidal signal

at the reference frequency. These quantities are checked visually against the eductor trace on the scope. Because of the first stage noise rejection, the LIA looks at a relatively noise-free signal, and the necessary manual adjustments

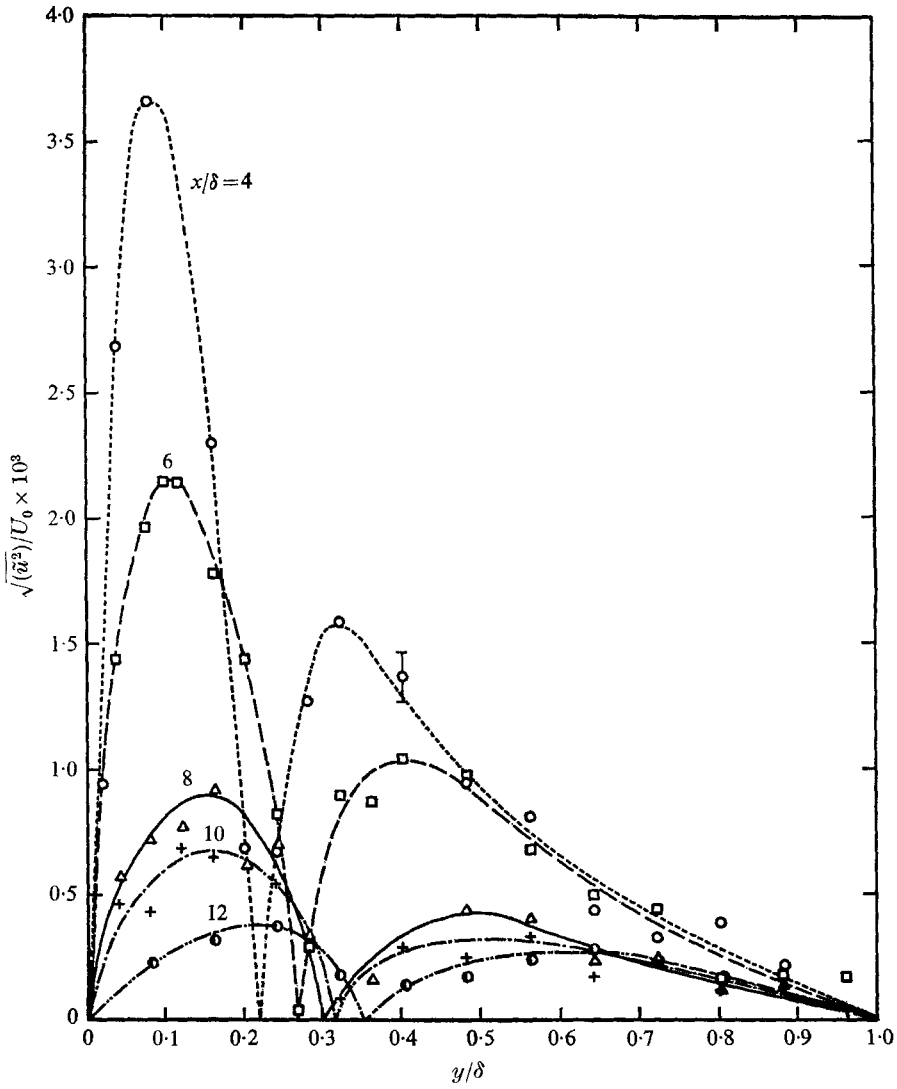

FIGURE 10. R.m.s. wave amplitude at 100 Hz, Re = 13,800. ○, x/δ = 4; □, x/δ = 6; △, x/δ = 8; +, x/δ = 10; ◐, x/δ = 12.

can be made in a very few seconds (after a period of about 20–30 min. for satisfactory eduction). Hence, *in toto* we obtain a picture of the waveform, and the amplitude and phase (relative to the ribbon voltage) of its fundamental component. The survey across the flow is repeated downstream from the ribbon at intervals of one channel width for as far as the signal can be detected.

5. Wave data and analysis

To date, data have been obtained at frequencies of 25, 50, 75 and 100 Hz, with the ribbons vibrating to produce a symmetric $\tilde{v}$ disturbance, which makes the streamwise disturbance ($\tilde{u}$) antisymmetric. Indeed, surveys across the channel centreline verified the antisymmetry of the $\tilde{u}$ osicllations. The 25 and 50 Hz

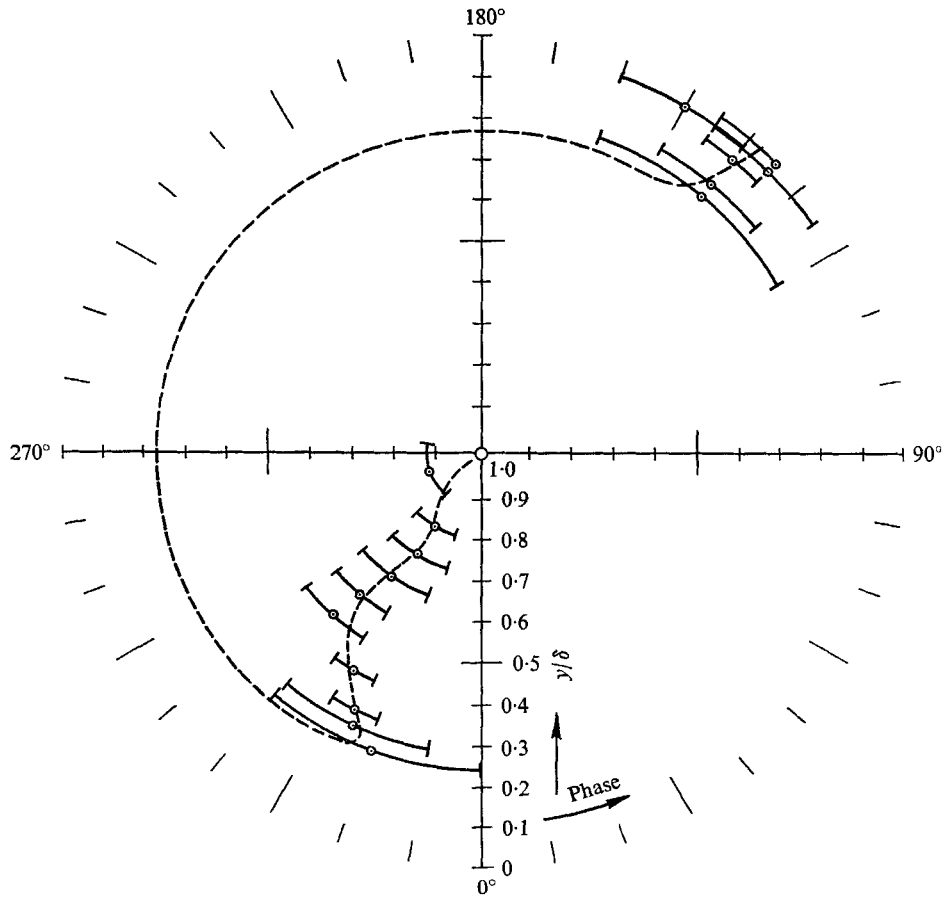

FIGURE 11. Wave phase at 100 Hz, Re = 13,800, x/δ = 4.
Bars denote phase uncertainties.

data appear to contain more than a single predominant eigenmode (the waveform is not very well preserved in the streamwise direction). The 100 Hz data most closely resemble excitation of a pure wave eigenmode, and we discuss only the 100 Hz data in this paper. All measurements reported here have been taken along the centre height of the channel. For other data, see Hussain (1970).

Figure 10 shows the distribution of the amplitude of the $\tilde{u}$ oscillation at several streamwise stations. The very small values of the amplitude emphasize the difficulty in detecting the organized wave and the need for a very large ensemble of wave oscillations. There appears to be a 180° phase reversal at a

point away from the wall, and in figure 10 we show zero $\tilde{u}$ to infer the phase reversal point. Where the amplitude is small, the phase uncertainty is very high. The uncertainty in amplitude is constant at all amplitudes, and hence is percentagewise substantial where the amplitude is small. The exact crossing point is therefore very difficult to define, and our best estimates are shown. Figure 11 shows the typical phase uncertainty distribution, and figure 12 the phase distribution at different stations.

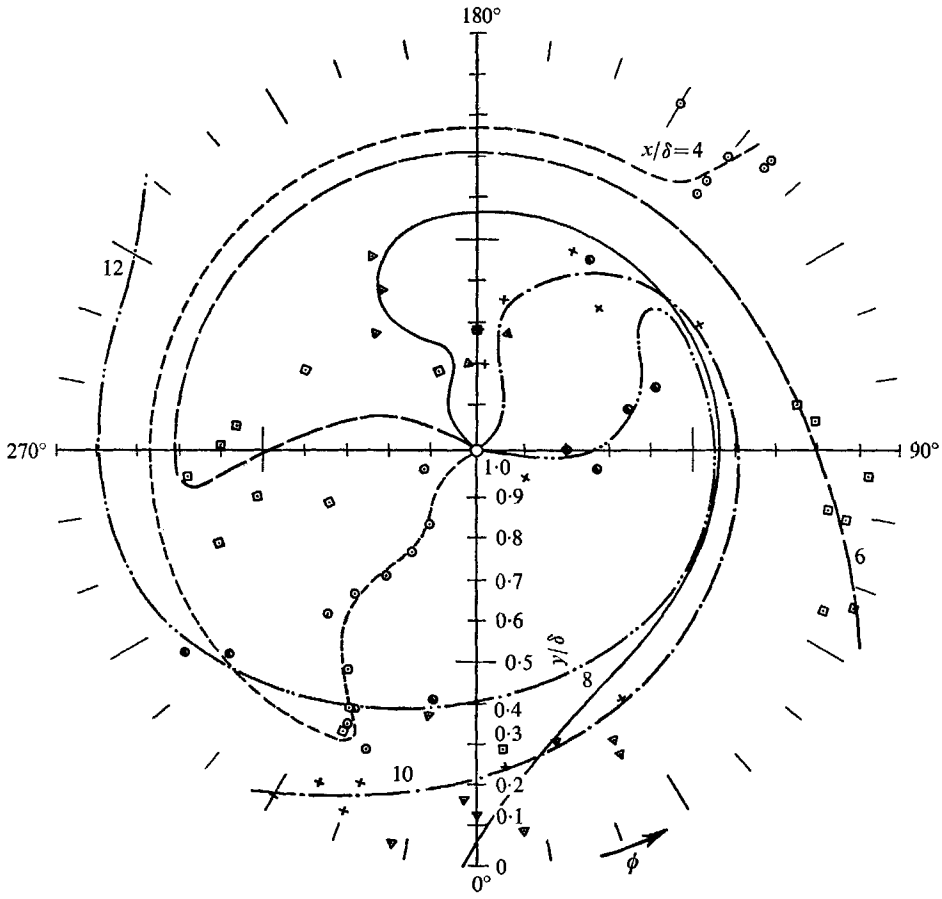

FIGURE 12. Wave phase at 100 Hz. Symbols same as figure 10.

Within these uncertainties, it remains clear that the waveform is not completely preserved, suggesting that the initial disturbance induced by the ribbon excites more than one of the wave eigenmodes corresponding to the excitation frequency. Figure 13 shows the decay in amplitude of the two peaks in the amplitude distribution and the amplitude change at two fixed positions away from the wall.

The phase data are not sufficiently accurate or complete to permit determination of the direction of the phase jump. Solutions of the inviscid Orr–Sommerfeld

equation show an increase in arg $(\tilde{u})$ of π at the critical layer, and hence we have drawn the phase curves counterclockwise at the phase jump.

A proper analysis of this data will require consideration of the multiple mode characteristics of the disturbance. Nevertheless, there is considerable interest in the results of a coarser analysis based on treatment of the disturbance as constituted by a single eigenmode. Let us suppose that the disturbance represents such a single mode and is of sufficiently small amplitude to be treated by linear theory. The two-dimensional disturbance velocities may then be written as

$$\tilde{\mathbf{u}} = \tfrac{1}{2}\{\hat{\mathbf{u}}(y)e^{i\alpha(x-ct)} + \hat{\mathbf{u}}^*(y)e^{-i\alpha^*(x-c^*t)}\}. \tag{5.1}$$

Here * denotes a complex conjugate, $\hat{\mathbf{u}} = (\hat{u}, \hat{v})$ is the eigenmode shape, $\alpha = \alpha_r + i\alpha_i$ the (complex) wave-number, α_r the spatial wave-number and α_i the spatial growth-factor, and c the wave speed. For convenience we treat all quantities as normalized on the mean velocity at the channel centreline (U_0) and the channel half-width (δ). Alternatively, we may put

$$\tilde{\mathbf{u}} = \tfrac{1}{2}\{\hat{\mathbf{u}}(y)e^{i(\alpha x-\omega t)} + \text{conjg}\}, \tag{5.2}$$

where ω is the (real) oscillation frequency. Within the approximations mentioned above, the data provide estimations of α, ω, c and $\tilde{u}(y)$. The continuity equation for two-dimensional waves becomes

$$i\alpha\hat{u} + \frac{d\hat{v}}{dy} = 0, \tag{5.3}$$

from which the cross-stream component $\tilde{v}$ can be calculated. This function is presumably the eigenfunction of an Orr–Sommerfeld-like equation containing (as yet unknown) terms accounting in a proper manner for the effect of the propagating wave oscillations on the background Reynolds stresses. Of additional interest is the Reynolds stress of the organized wave,

$$-\overline{\tilde{u}\tilde{v}} = -\tfrac{1}{4}(\hat{u}\hat{v}^* + \hat{u}^*\hat{v}). \tag{5.4}$$

This can be obtained once $\hat{v}$ has been calculated.

Starting with (5.2), one may easily show that α_i can be deduced from the measured oscillation amplitudes at two streamwise stations x_1 and x_2, using

$$\frac{|\tilde{u}|_{x_2, y}}{|\tilde{u}|_{x_1, y}} = e^{-\alpha_i(x_2-x_1)}. \tag{5.5}$$

If the wave-shape is preserved, it does not matters at what y position the amplitudes are determined. Some variation in α_i is obtained from the data of figure 13, depending on the point y chosen. A reasonable average is

$$\alpha_i = 0{\cdot}27.$$

Again starting with (5.2), denoting the measured phases of $\tilde{u}$ (relative to the wave-maker reference) at (x_1, y) and (x_2, y) by ϕ_1 and ϕ_2, one finds that

$$\alpha_r = \frac{\phi_2 - \phi_1}{x_2 - x_1}. \tag{5.6}$$

Here more interpretation is required. Inspection of the lower frequency data suggests that the phase difference per survey station (per gap width) is about 430°. This yields

$$\alpha_r = 3{\cdot}7,$$

corresponding to a wavelength of about 2·1 in. The centreline velocity at $Re = 13{,}800$ is 21·9 ft./sec, so the dimensionless frequency at $f = 100$ Hz is

$$\omega = 2\pi f\delta/U_0 = 3{\cdot}0.$$

Hence, the normalized wave-speed is

$$c = \omega/\alpha = 0{\cdot}81 - i0{\cdot}02.$$

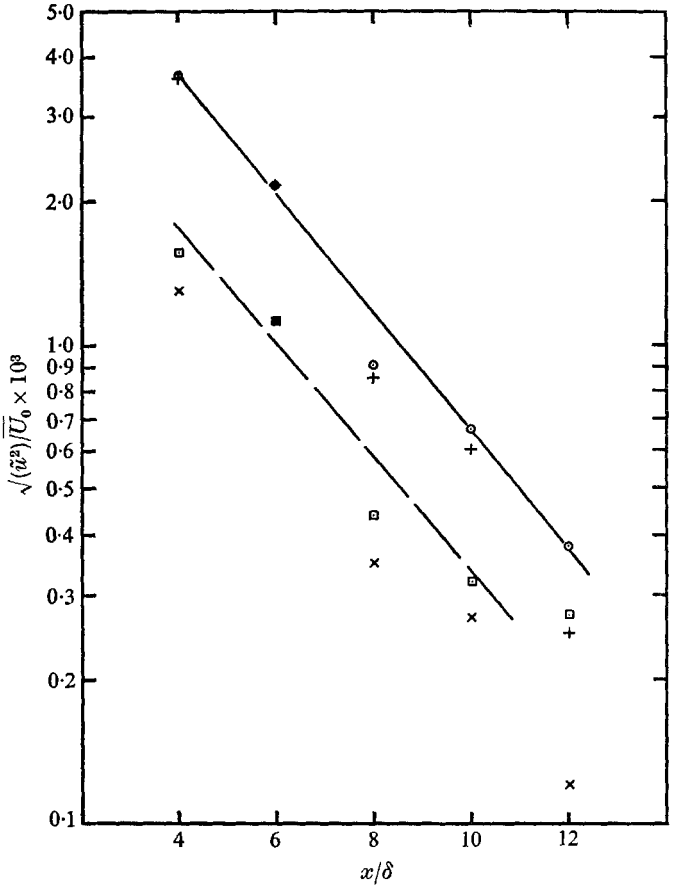

FIGURE 13. Spatial decay of amplitude. ⊙, peak near wall; ⊡, outer peak; +, $y/\delta = 0{\cdot}1$; ×, $y/\delta = 0{\cdot}4$; $Re = 13{,}800$, $n = 100$ Hz.

The $\tilde{v}$ distribution has been calculated by numerical integration, using (5.3) and smoothed data for $\tilde{u}$ at each survey station. The amplitude and phase distribution of the calculated $\tilde{v}$ distribution are shown in figure 14 and figure 15. The spatial decay rate of $\tilde{v}$ at its peak and at constant distance from the wall is shown in figure 16. The decay rate is comparable with that of $\tilde{u}$. Normalization

on the centreline value of $\tilde{v}$ was frustrated by the inaccuracy in the phase data at that point, and hence we show the $\tilde{v}$ amplitude and phase at each station as computed from the interpreted $\tilde{u}$ data. Note that the five profiles are of generally similar shape, and that at the last three stations the curves are quite similar in both amplitude and phase. These three curves might be interpreted as arising from the fundamental wave eigenmode, which should have an eigenvalue of about $\alpha = 3{\cdot}7 + 0{\cdot}27i$ at $\omega = 3{\cdot}0$, $Re = 13{,}800$. With some reservation we offer this as a

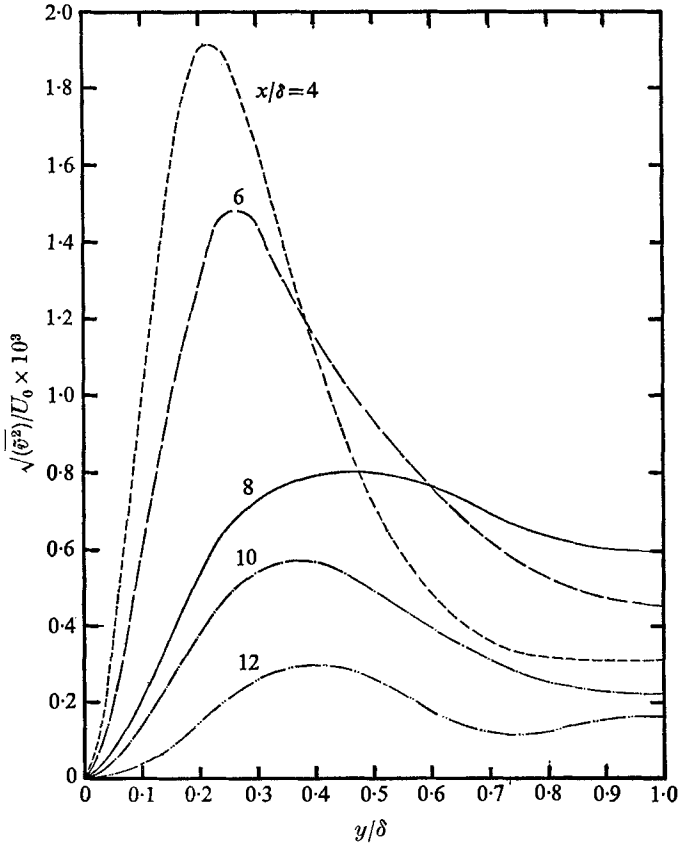

FIGURE 14. Calculated r.m.s. $\tilde{v}$ distribution. Symbols same as figure 10.

target for Orr–Sommerfeld analysis in turbulent shear flows. It is clear that the peaks in $\tilde{u}$ and $\tilde{v}$, and the cross-over point in $\tilde{u}$ move away from the wall progressively with downstream stations. The drift of the disturbances away from the wall is shown in figure 17.

The Reynolds stress distributions computed as described above are shown in figure 18. There is considerable uncertainty in the shape of these curves arising from the interpretation of arg ($\hat{u}$) and this is reflected in the differences between the five curves. These distributions should not be taken very seriously at present, and we include them simply for completeness.

Calculations based on the Orr–Sommerfeld equation and a similar equation

modified to include the oscillations in the background Reynolds stresses through the basic flow eddy viscosity have been carried out for the experimental mean profile. The numerical methods (Lee & Reynolds 1967) and the eddy viscosity profile used (Reynolds & Tiederman 1967) are described elsewhere. Neither model is at all successful in predicting $\hat{u}$ as interpreted above. The quasi-laminar model ($\tilde{r}_{ij} = 0$) shows too many peaks, and the model based on the variable mean eddy viscosity does not show the two peaks. The eigenvalues are relatively

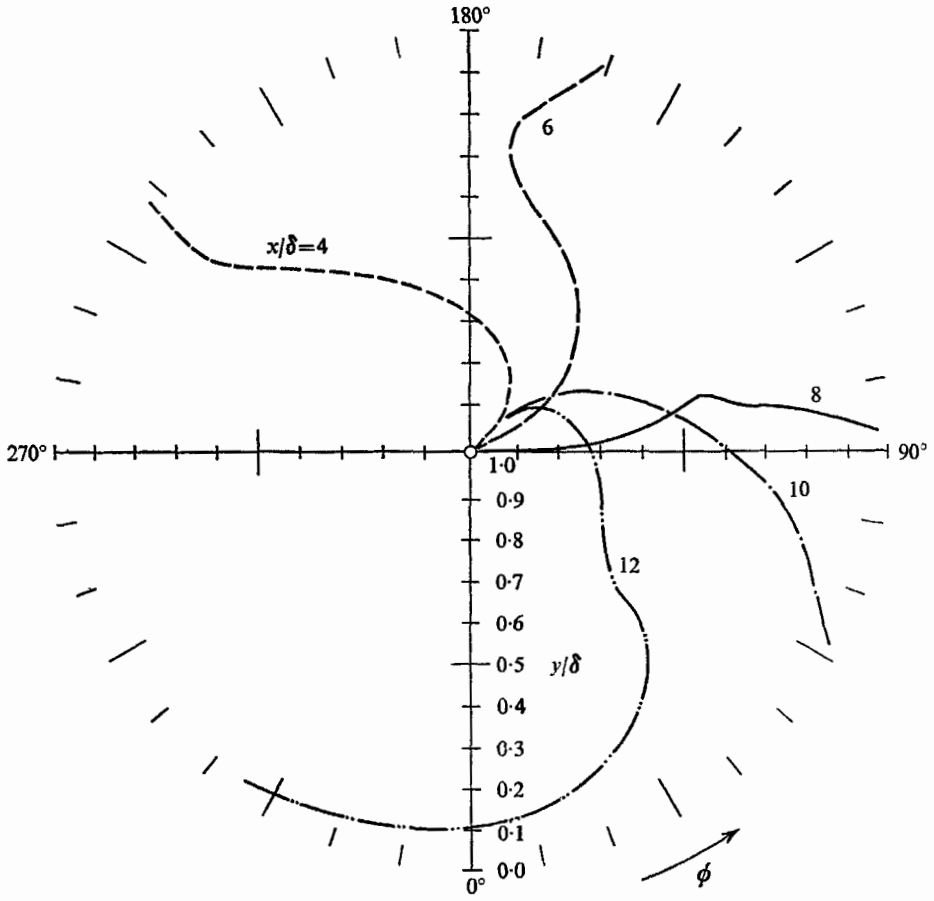

FIGURE 15. Calculated $\tilde{v}$ phase. Symbols same as figure 10.

similar, with that for the eddy viscosity model being somewhat closer to the experimental value. In particular, the trends of wave speed with frequency are incorrectly predicted by the quasilaminar model, while the eddy viscosity model at least gives the correct trends. It is clear that neither is suitable, and that more fundamental work on the theory, as well as further experimentation, is required.

This work was supported by the National Science Foundation and the U.S. Air Force Office of Scientific Research.

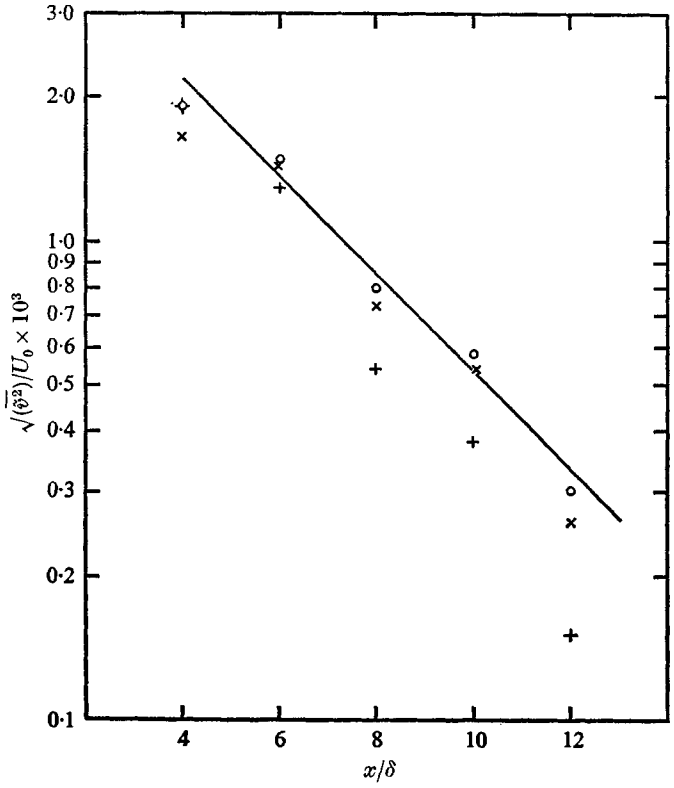

FIGURE 16. Spatial decay of calculated r.m.s. $\tilde{v}$.
○, peak; +, $y/\delta = 0{\cdot}2$; ×, $y/\delta = 0{\cdot}3$.

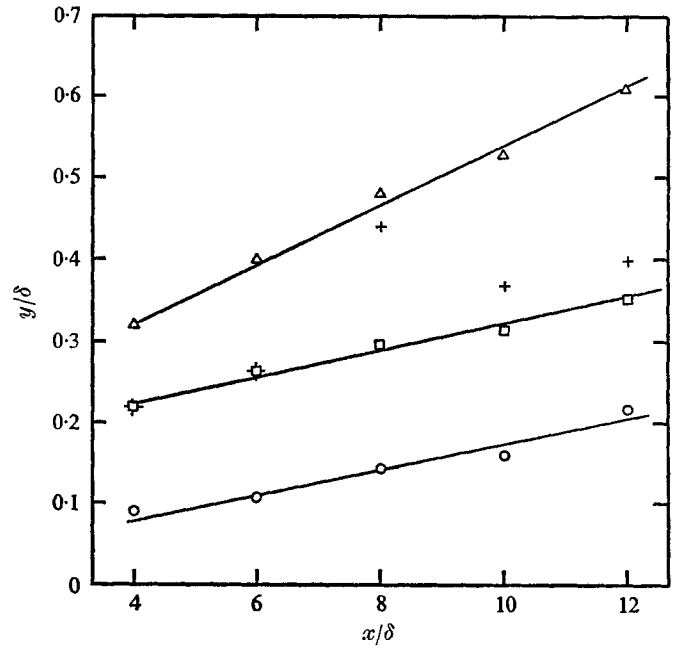

FIGURE 17. Drift of disturbances away from wall. ○, wall $|\tilde{u}|$ peak;
□, $|\tilde{u}| = 0$; △, outer $|\tilde{u}|$ peak; +, $|\tilde{v}|$ peak.

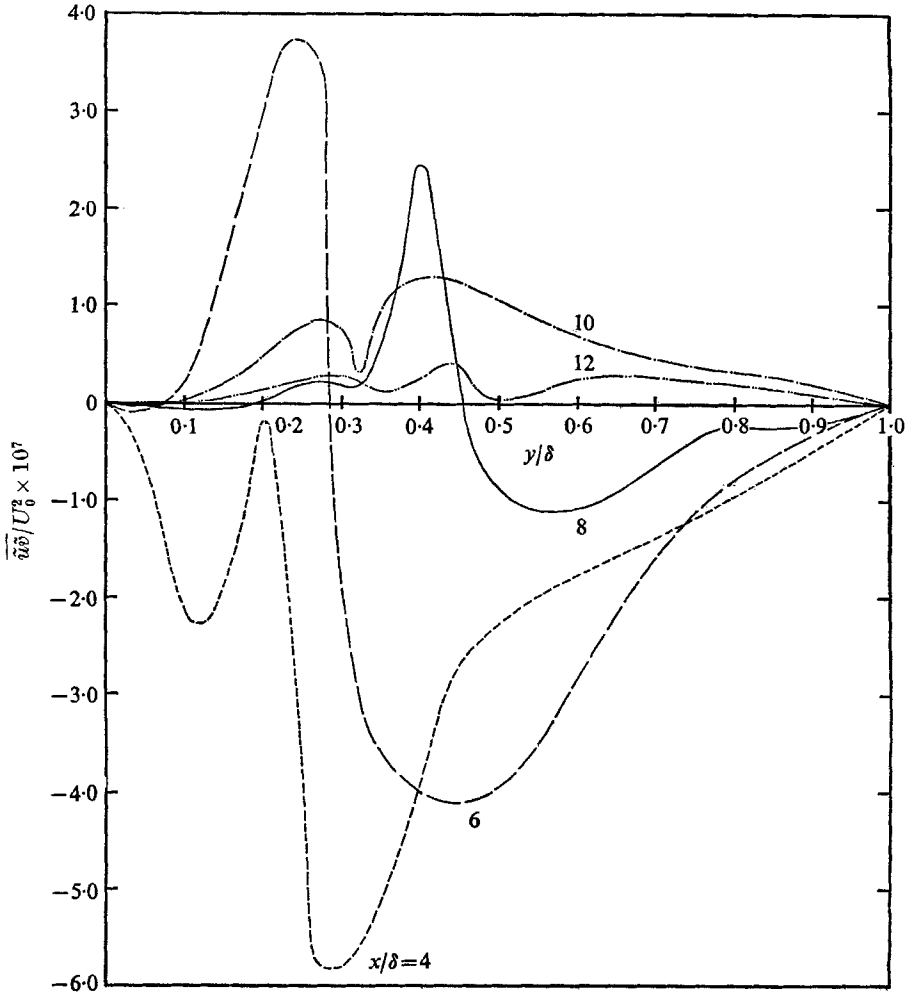

FIGURE 18. Calculated Reynolds stress distribution. Symbols same as figure 10.

REFERENCES

BAKEWELL, H. P. & LUMLEY, J. 1967 *Phys. Fluids*, **10**, 1880.

CLARK, J. A. 1968 *Trans. ASME (J. Basic Eng.)*, December, 1968.

COLES, D. E. 1956 *J. Fluid Mech.* **1**, 191.

COMTE-BELLOT, G. 1963 Contribution a l'etude de la turbulence de conduite. Doctoral Thesis, University of Grenoble.

HUSSAIN, A. K. M. F. 1970 Mechanics of perturbation waves in turbulent channel flow. Ph.D. Thesis, Stanford University.

LANDAHL, M. T. 1967 *J. Fluid Mech.* **29**, 441.

LAUFER, J. 1951 *NACA Rep.* 1058.

LAUFER, J. 1954 *NACA Rep.* 1174.

LEE, L. & REYNOLDS, W. C. 1967 *Quart. J. Mech. Appl. Math.* **20**, 1.

LUMLEY, J. 1967 *Proc. Int. Colloq. on Atm. Turb. and Radio Wave Prop.* Moscow.

MORRISON, W. R. B. & KRONAUER, R. E. 1968 *Proc. 12th Int. Cong. Appl. Mech.*

PHILLIPS, O. M. 1967 *The Dynamics of Upper Ocean.* Cambridge University Press.

REYNOLDS, W. C. & TIEDERMAN, W. G. 1967 *J. Fluid Mech.* **27**, 253.